npj | clean water

www.nature.com/npjcleanwater

ARTICLE OPEN

Check for updates

Breaking interfacial charge transfer barrier by sulfite for efficient pollutants degradation: a case of $BiVO_4$

Xin Gao[1], Peifang Wang[1]✉, Huinan Che[1], Wei Liu[1] and Yanhui Ao[1]✉

Heterogeneous photocatalytic systems generally lack thermodynamic dependence on the degradation of organic pollutants in aqueous solution. Therefore, it is important to reveal the reasons for the inhibited surface kinetics but still be neglected. Herein, we reveal the mechanism that $BiVO_4$ can't degrade organics although it is thermodynamically feasible. The surface solvation and formation of double layer (compact layer and diffuse layer) makes low-polarity organics far away from the surface of $BiVO_4$. We found that the introduction of sulfite can solve this problem. Theory calculation illustrates that sulfite can enter into the compact layer because of its higher adsorption energy on $BiVO_4$ and lower adiabatic ionization potential (AIP). Then, photogenerated holes initiate the chain transformation of sulfite and produce strong oxidizing species which can diffuse out to degrade organics. This paper provides an insight into the understand the effects of solid-liquid interface on heterogeneously photocatalytic degradation of organic pollutants.

npj Clean Water (2023)6:42 ; https://doi.org/10.1038/s41545-023-00254-w

INTRODUCTION

Heterogeneous photocatalysis is considered as the potential strategy for water decontamination due to its high efficiency, environmental benignity, cost effectiveness, and potential utilization of solar energy[1,2]. The photocatalytic reaction mechanisms can be mainly divided into radical and non-radical pathways. Radical-type photocatalysts can generate hydroxyl radical (•OH) under light irradiation and form a gradient distribution of radical at the solid-liquid interface[3]. Meanwhile, the reactivity of •OH is independent of its production method, leading to its high reactivity and the universality of organic degradation[1]. In contrast, the holes generated by non-radical-type photocatalysts are only localized on the surface to undergo redox reactions. Compared with radical systems, the reactivity of non-radical-type photocatalysts towards organic molecules is more complicated. In particular, $BiVO_4$, as a typical non-radical-type photocatalyst, exhibits inhibited surface kinetics for the degradation of organic molecules including phenol, ciprofloxacin, and sulfonamides[4–7]. However, although the photogenerated hole of $BiVO_4$ has higher redox potential (ca. +2.5 V vs. NHE)[8], the active species [•OH (+1.8 ~ 2.7 V vs. NHE)[9], high-valent metal-oxo[10–12] and singlet oxygen ($^1O_2$, +1.88 V vs. NHE)[13] with lower redox potentials generated in advanced oxidation processes exhibit higher rate constant for organics[3,14]. It suggests a contradiction between the reactivity of non-radical-type photocatalytic system for organics and the ideal photocatalytic model controlled by thermodynamics. Generally, similar to the overpotential theory, the redox potential of photogenerated holes should be positively correlated with the oxidation reaction trend of organic molecule. Therefore, under the satisfied thermodynamic conditions, the reason why organic molecules are difficult to be degraded by non-radical-type heterogeneous photocatalytic system may be the limited interface reaction kinetics. According to kinetic theory, solvation is a key influencing factor in aqueous reactions. Among them, the stabilization of the reactants by the solvation effect will significantly increase the activation energy of the reaction. In particular, the holes of non-radical photocatalysts belong to short-range active species, which can only oxidize the molecules on the surface. The results of first-principles and ab initio molecular dynamics studies show that water molecules mainly exist in two interface interaction modes on the most stable (010) plane of $BiVO_4$: water molecules coordinating with Bi^{3+} sites through lone pair electrons and interacting with oxygen terminal of VO_4 tetrahedron through hydrogen bonds[15–17]. Strong $BiVO_4$-water interface interaction may significantly reduce the reaction rate of photogenerated holes with organic molecules. However, the influence of solvation effects on the degradation efficiency of organics in non-radical-type heterogeneous photocatalytic systems is seriously neglected. Therefore, it is necessary to further explore the effect of solid–liquid interface on the organic degradation kinetics in the non-radical-type photocatalytic system and decrease the interfacial electron transfer barrier from organic molecule to photocatalyst.

In various strategies to improve interfacial electron transfer, sulfite can effectively trap the photogenerated holes of the photocatalyst to generate active radicals (e.g., $SO_3^{\bullet-}$, $SO_5^{\bullet-}$, $SO_4^{\bullet-}$, •OH), which can promote the gradient distribution of active species at the solid-liquid interface and the degradation of organic molecules[18,19]. For example, Deng et al. found that BiOBr combined with 20 mM sulfite could completely degrade 20 mg L^{-1} methyl orange within 30 min under visible light[20]. Wei et al. combined g-C_3N_4 with sulfite under visible light to significantly improve the removal performance of organic dyes and phenol[21]. However, in previous reports, the solid-liquid interface structure, interaction mode between sulfite and photocatalysts, and the photocatalytic activation law of sulfite have not been thoroughly elucidated.

Sulfamethoxazole (SMX) are the oldest group of antibiotics used in human and veterinary medicines for bacterial infections treatment. Considering its polarity, amphotericity, photo- and thermal stability, SMX has a high migration ability in the environment, which has become an emerging issue and potential

[1]Key Laboratory of Integrated Regulation and Resource Development on Shallow Lakes, Ministry of Education, College of Environment, Hohai University, No.1, Xikang road, Nanjing 210098, China. ✉email: pfwang2005@hhu.edu.cn; andyao@hhu.edu.cn

threat to marine life and human health. Searching for suitable methods with high-efficiency degradation of SMX is one of the most challenging missions. Herein, we achieved sulfite-mediated indirect interfacial electron transfer between $BiVO_4$ and organic molecules. The differences in interfacial interaction and electron transfer of sulfite and SMX on the surface of $BiVO_4$ were explored by electrochemistry and theoretical calculations, while their existence mode at the solid-liquid interface was revealed. Furthermore, the chain transformation of sulfite at the solid-liquid interface was confirmed by quenching experiments and electron spin resonance (ESR). Finally, combined with semiconductor physics, interfacial chemistry, and double-layer theory, the role of sulfite in the interfacial electron transfer of the non-radical $BiVO_4$ photocatalytic system is elaborated.

RESULTS

Oxidation kinetics of SMX in the $Na_2SO_3/BiVO_4$ system

According to the structural characterization (Supplementary Figs. 1–5), $BiVO_4$ is a monoclinic decahedral structure with exposed (010)/(110) facets, which has an excellent visible light response. However, no change in SMX concentration is recorded in the presence of $BiVO_4$ under visible light (Fig. 1), which indicates the limited kinetics of SMX degradation on the surface of $BiVO_4$. Furthermore, the photolysis of SMX in the absence of photocatalysts can be neglected, due to its lack of visible light absorption[22]. Since the chain transformation of sulfite (Na_2SO_3) is difficult to trigger under visible light, SMX is not degraded in the presence of sulfite alone. In contrast, once 0.5 mM sulfite is added to the photocatalytic system of $BiVO_4$, SMX exhibits a rapid degradation with a removal efficiency of 85.6% within 15 min. Therefore, it is necessary to further explore the sulfite-mediated mechanism and predominant active species in the $Na_2SO_3/BiVO_4$ system.

Mechanism on sulfite activation in the system

According to the activation mechanism, sulfite is converted to a $SO_3^{\bullet-}$ via one-electron oxidation (Eq. 1)[20]. Since the ground-state O_2 is a double-radical with triplet state, it will rapidly add to the $SO_3^{\bullet-}$ to form $SO_5^{\bullet-}$ (Eq. 2)[18,23,24]. Subsequently, $SO_5^{\bullet-}$ is reduced by $SO_3^{\bullet-}$ into peroxymonosulfate (PMS) and $SO_4^{\bullet-}$ (Eqs. 3, 4)[23].

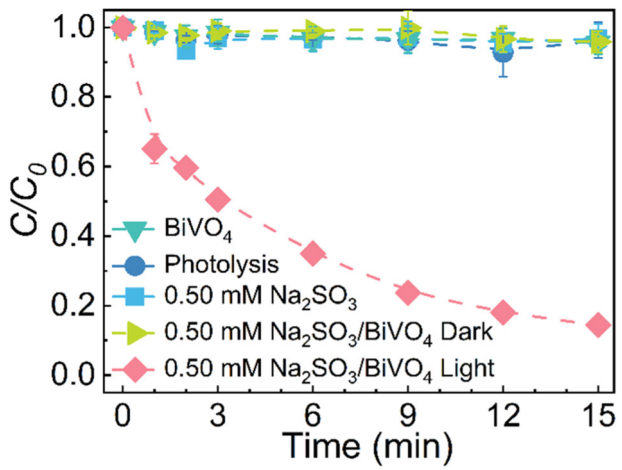

Fig. 1 Kinetics of interfacial reaction of $BiVO_4$ activated by sulfite. Degradation of SMX by $BiVO_4$, Na_2SO_3, $Na_2SO_3/BiVO_4$, and blank systems under visible light. Experimental conditions: [SMX] = 4 μM, [Na_2SO_3] = 0.50 mM, [$BiVO_4$] = 1.0 g L^{-1}, initial pH = 7.0, $\lambda \geq 420$ nm, and $T = 25$ °C. The center of the data point is the mean of the two sets of data, and error bars represent the standard deviation of the two sets of data.

Among them, $SO_4^{\bullet-}$ with the high redox potential can further oxidize H_2O/OH^- to generate •OH (Eqs. 5, 6)[23]. Therefore, $SO_3^{\bullet-}$, $SO_5^{\bullet-}$, $SO_4^{\bullet-}$ and •OH may be formed in the $Na_2SO_3/BiVO_4$ system.

$$SO_3^{2-} + h^+(BiVO_4) \rightarrow SO_3^{\bullet-} \quad (1)$$

$$SO_3^{\bullet-} + O_2 \rightarrow SO_5^{\bullet-} \quad (2)$$

$$SO_5^{\bullet-} + SO_3^{2-} \rightarrow SO_4^{\bullet-} + SO_3^{2-} \quad (3)$$

$$SO_5^{\bullet-} + SO_3^{2-} \rightarrow SO_5^{2-} + SO_3^{\bullet-} \quad (4)$$

$$SO_4^{\bullet-} + H_2O \rightarrow SO_4^{2-} + \bullet OH + H^+ \quad (5)$$

$$SO_4^{\bullet-} + OH^- \rightarrow SO_4^{2-} + \bullet OH \quad (6)$$

$$SO_4^{\bullet-} + SO_3^{2-} \rightarrow SO_4^{2-} + SO_3^{\bullet-} \quad (7)$$

$$\bullet OH + SO_3^{2-} \rightarrow SO_3^{\bullet-} + OH^- \quad (8)$$

Initially, the photocatalytic degradation of SMX by $BiVO_4$ in the presence of sulfite under different atmospheres is carried out. From Fig. 2a, SMX has the highest degradation performance under the condition of air purging, while the dissolved oxygen (DO) concentration is rapidly consumed to the lowest at the initial reaction stage (Supplementary Fig. 6). After that, due to stirring and air purging, the DO concentration gradually increases. According to the sulfite activation mechanism, O_2 only can be consumed by $SO_3^{\bullet-}$, implying that sulfite is rapidly oxidized at the initial reaction stage. Furthermore, the degradation rates of SMX slightly decrease without air purging, indicating that higher DO concentration is conducive to the production of active species. In addition, under anaerobic conditions (Ar purging), the degradation of SMX can be neglected, demonstrating that O_2 acts as the initiator of the active species generation and SMX is difficult to be oxidized by $SO_3^{\bullet-}$.

To further investigate the active species generation, quenching experiments and ESR were performed. Since $SO_4^{\bullet-}$ are more sensitive to α-H, the rate constant (k) of tert-butyl alcohol (TBA) and ethanol (EtOH) with $SO_4^{\bullet-}$ [$k_{TBA,SO_4^{\bullet-}} = (4.0-9.1)\times 10^5 M^{-1}s^{-1}$, $k_{EtOH,SO_4^{\bullet-}} = (1.6-7.7)\times 10^7 M^{-1}s^{-1}$] are quite different, while •OH have less effect [$k_{TBA,\bullet OH} = 6.0\times 10^8 M^{-1}s^{-1}$, $k_{EtOH,\bullet OH} = 1.9\times 10^9 M^{-1}s^{-1}$][11,25]. As observed in Fig. 2b, the addition of TBA (1 mM and 10 mM) just slightly retarded the oxidation of SMX. Significant inhibitory action can be observed only when TBA concentration is increased to 100 mM. In contrast, there is a strong inhibition with the addition of 1 mM EtOH, and the inhibitory effect gradually enhance with the increase of EtOH concentration (Fig. 2c). Therefore, $SO_4^{\bullet-}$ may be the major active species in the $Na_2SO_3/BiVO_4$ system ($k_{SMX,SO_4^{\bullet-}} = 0.93\times 10^9 M^{-1}s^{-1}$)[26], while •OH play an auxiliary role ($k_{SMX,OH} = 6.78\times 10^9 M^{-1}s^{-1}$)[12]. In addition, ESR was carried out to probe the production of active species (Fig. 2d). Strangely, there is a distinct signal of DMPO-•OH in the $BiVO_4$ system under visible light, which opposite to the degradation of SMX in the $BiVO_4$ system ($k_{SMX,\bullet OH} = 6.78\times 10^9 M^{-1}s^{-1}$). This may originate from the hole-assisted H_2O nucleophilic attack for DMPO (Supplementary Fig. 7a), but does not actually generate •OH[25]. When sulfite is added to $BiVO_4$ suspension, the signal of DMPO-•OH was further enhanced, indicating that the introduction of sulfite significantly promoted the generation of strong oxidative radicals. However, the DMPO-$SO_4^{\bullet-}$ adduct signal is not clearly detected, which may be attributed to the poor stability of DMPO-$SO_4^{\bullet-}$ and easy decomposition to DMPO-•OH (Supplementary Fig. 7b)[25]. In addition, $SO_5^{\bullet-}$ are also produced during the chain transformation of sulfite. However, according to previous reports, $SO_5^{\bullet-}$ has weak reactivity, indicating that $SO_5^{\bullet-}$ almost did not take part in the degradation process of SMX[23]. Therefore, we can conclude that $SO_4^{\bullet-}$ is the predominant active species for SMX

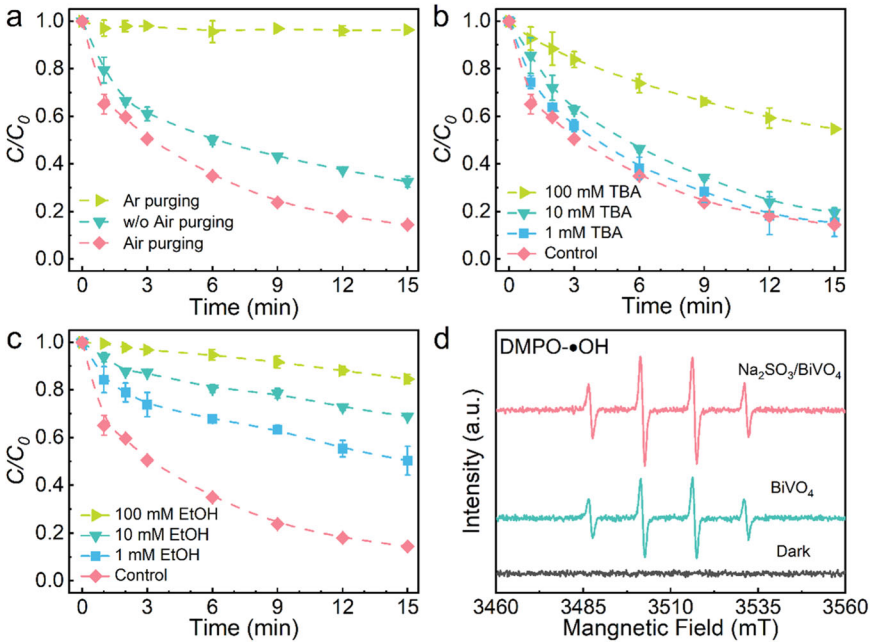

Fig. 2 Dominated active species for SMX degradation in the Na_2SO_3/$BiVO_4$ system. **a** Degradation of SMX in different atmosphere conditions. Effects of **b** TBA and **c** EtOH on SMX degradation in the Na_2SO_3/$BiVO_4$ system; **d** ESR signals for the detection of reactive species generated in the Na_2SO_3/$BiVO_4$ system. Experimental conditions: **a** [SMX] = 4 μM, [Na_2SO_3] = 0.50 mM, [$BiVO_4$] = 1.0 g L^{-1}, [TBA] = 1–100 mM, [EtOH] = 1–100 mM, [DMPO] = 100 mM, initial pH = 7.0, $\lambda \geq 420$ nm, and $T = 25$ °C. The center of the data point is the mean of the two sets of data, and error bars represent the standard deviation of the two sets of data.

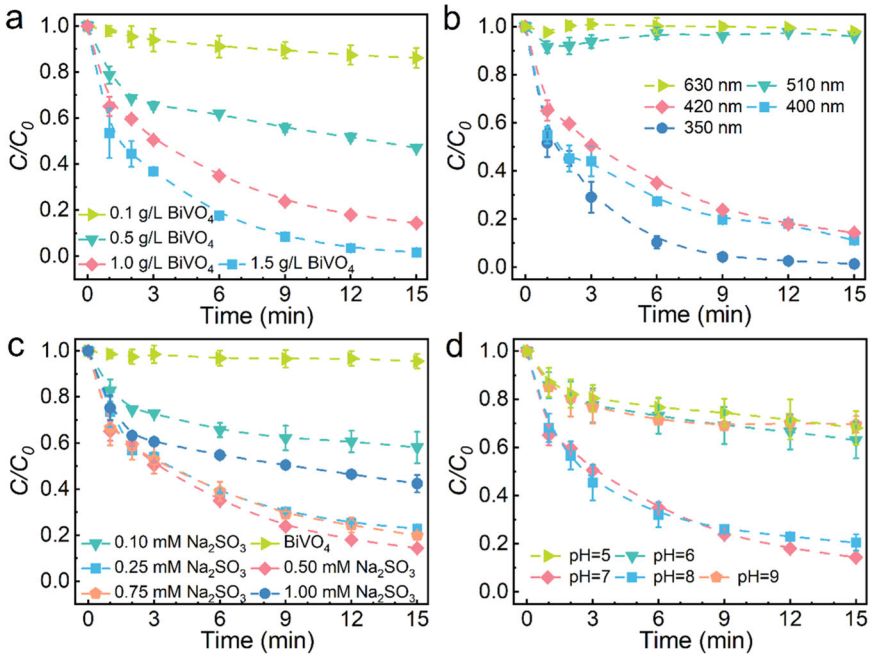

Fig. 3 Controlled experiment. Effect of **a** $BiVO_4$ concentration, **b** light irradiation range, **c** Na_2SO_2 concentration, and **d** pH on the degradation of SMX. Experimental conditions: [SMX] = 4 μM, [Na_2SO_3] = 0.50 mM, [$BiVO_4$] = 1.0 g L^{-1}, initial pH = 7.0, $\lambda \geq 420$ nm, and $T = 25$ °C. The center of the data point is the mean of the two sets of data, and error bars represent the standard deviation of the two sets of data.

degradation in the Na_2SO_3/$BiVO_4$ system, while the contribution from •OH, $SO_5^{\bullet-}$, $SO_3^{\bullet-}$ is driven to a lesser extent.

The mechanism of sulfite activation by $BiVO_4$ under visible light was further explored by control experiments. It could be seen from Fig. 3a that with the increase of $BiVO_4$ concentration, the degradation performance of SMX is gradually improved, implying that the higher reactive surface area of $BiVO_4$ is conducive to the increase of $SO_4^{\bullet-}$ generation proportion. Meanwhile, there is an observe obvious wavelength dependence of light irradiation in the Na_2SO_3/$BiVO_4$ system (Fig. 3b). This due to the blue-shift of the cutoff wavelength increasing the carrier concentration of $BiVO_4$. Moreover, the degradation performance of SMX display a volcanic relationship with the change of sulfite concentration (Fig. 3c). This may originate from that excessive sulfite will quench the active

species (e.g., $SO_4^{\bullet-}$ and •OH) (Eqs. 7, 8). In summary, under the consistent of sulfite concentration, the increase of $BiVO_4$ concentration and the blue-shift of the cutoff wavelength promotes the higher proportion of $SO_4^{\bullet-}$ production. Meanwhile, there is an optimal dosage of sulfite under the consistent of the $BiVO_4$ concentration and light irradiation conditions. Wherein, insufficient sulfite reduced the yield of active species, and excessive sulfite produced a stronger self-quenching effect. According to DO (Supplementary Fig. 6) and pH (Supplementary Fig. 8) change of solution, it can be seen that a large amount of sulfite is consumed at the initial reaction stage. This indicates that the higher proportion of sulfite oxidation at the initial stage will be conducive to the generation of strong oxidative radicals ($SO_4^{\bullet-}$ and •OH). In addition, the $Na_2SO_3/BiVO_4$ system presents obvious pH dependence (Fig. 3d), and displays highest degradation performance for SMX under neutral conditions. Wherein, under acidic conditions, the protonation of sulfite enhances its ionization potential and inhibits its activation (Supplementary Table 1). It could be seen from Supplementary Figs. 9, 10 that under alkaline conditions, $BiVO_4$[27], SO_3^{2-} and SMX are all negatively charged, which increases the electrostatic repulsion among $BiVO_4$, SMX, and $SO_4^{\bullet-}$, resulting in inhibition of SMX degradation.

Investigation of the interface reaction

The interfacial reaction of sulfite on the surface of $BiVO_4$ was further investigated by chopping LSV. As revealed in Fig. 4, the current density of $BiVO_4$ gradually enhances with the increase of positive bias voltage under visible light, which displays the excellent photoelectrochemical properties of $BiVO_4$. However, when SMX was added to the solution, the current density of $BiVO_4$ is obviously suppressed, indicating that SMX is difficult to undergo oxidation by direct electron transfer on the surface of $BiVO_4$. Interestingly, the current curve of $BiVO_4$ is drastically red-shifted and its current density is essentially increased with the addition of sulfite, which indicates that the holes of $BiVO_4$ can be effectively trapped by sulfite. When SMX was further added to the electrolyte, the current density is further enhanced, indicating that SMX, as a receptor of $SO_4^{\bullet-}$, significantly promoted the interface electron transfer of $BiVO_4$.

Mechanism of interface reaction in the $BiVO_4$ photocatalytic system

The photoexcitation of $BiVO_4$ and the interfacial interaction between sulfite and $BiVO_4$ were investigated by theoretical

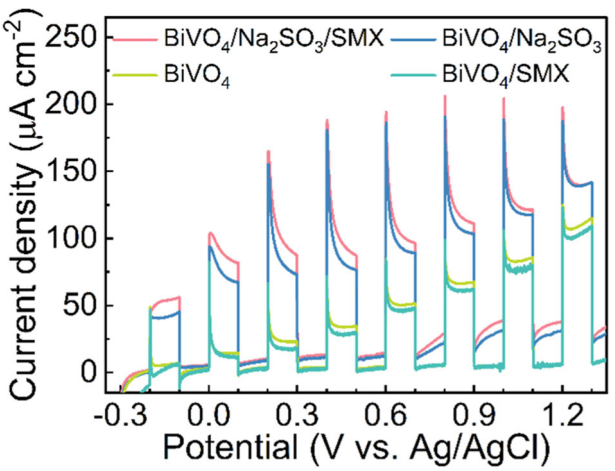

Fig. 4 Photoelectrochemical experiment. Photocurrent linear sweep voltammetry (LSV) scan of $BiVO_4$ photoanodes with Na_2SO_3 and SMX (0.1 M Na_2SO_4, [Na_2SO_3] = 0.5 mM, [SMX] = 4 μM, pH = 7.0) under chopped illumination ($\lambda = 510 \pm 60$ nm).

calculations. Figure 5a and Supplementary Fig. 11 illustrates the valence band (VB) of $BiVO_4$ is mainly composed of hybrid orbitals of Bi_{6s} and O_{2p}, while its conduction band (CB) is mainly composed of V_{3d}, indicating that the Bi-O structure acts as the region where holes principally accumulate[28]. Meanwhile, the valence band top of $BiVO_4$ composed of Bi6s orbitals reduces the effective mass of holes and increases the mobility, which effectively promotes the surface oxidation reaction. Fortunately, the (110) plane of $BiVO_4$ is mainly composed of Bi-O layers, forming the hole gathering plane (Fig. 5c). As shown in Fig. 5c and Supplementary Table 2, sulfite has higher adsorption energy and charge transfer amount on the surface of $BiVO_4$ compared with SMX (Supplementary Fig. 12). In addition, sulfite has a lower adiabatic ionization potential (AIP) than that SMX (Supplementary Table 1), indicating that sulfite is more prone to one-electron oxidation. In summary, there is a strong coupling effect between adsorption and single-electron oxidation of sulfite on the surface of $BiVO_4$.

According to the above experimental and theoretical analysis results, the interaction and reaction of sulfite and SMX on the surface of $BiVO_4$ can be summarized. The main active species for the degradation of organic molecules in the photocatalytic system include superoxide radical ($\bullet O_2^-$), hydroxyl radical (•OH), and hole (h^+). The contribution of $\bullet O_2^-$ to the degradation of organic molecules is excluded due to its weak oxidation, while •OH is not generated in the $BiVO_4$ photocatalytic system. Therefore, photogenerated holes are the only active species in the $BiVO_4$ photocatalytic system. In particular, h^+ belonging to short-range active species can only oxidize molecules in the compact layer[3]. According to the ideal photocatalysis model, the non-radical pathway of the photocatalysis system includes diffusion of organic molecules to the photocatalyst surface, reaction with photogenerated h^+, and desorption into bulk solution. Simultaneously, the thermodynamics of surface reaction is determined by the potential difference between the photogenerated h^+ and organic molecules. The higher the overpotential, the stronger the reaction trend. According to previous reports, the top of the valence band of $BiVO_4$ is ~2.5 V vs. NHE[8]. Compared with $BiVO_4$, the active species [•OH (+1.8 ~ 2.7 V vs. NHE)[9], high-valent metal-oxo[10–12] and $^1O_2$ (+1.88 V vs. NHE)[13]] with lower redox potential exhibit higher reactivity to organic molecules. And graphitic carbon nitride (g-C_3N_4), which is also a photocatalyst, has only the position of valence band of 1.5–2.0 V vs. NHE[29,30], showing excellent SMX degradation performance[31]. Therefore, the limited SMX degradation reaction of $BiVO_4$ might be controlled by kinetics. Especially, the identification of the difference between g-C_3N_4 and $BiVO_4$ can better reflect the kinetic control effect in the heterogeneous photocatalytic system. From the structural point of view, the surface of $BiVO_4$ is composed of oxygen terminal or hydroxyl group, because both Bi^{3+} and V^{5+} are extremely oxyphilic. However, g-C_3N_4 formed from thermal polymerization is relatively weak in hydrophilicity, and its structure is a heptazine-ring conjugated organic polymer linked by amino nitrogen[32]. Therefore, g-C_3N_4 lacking surface hydrophilic groups are less bound to surface water molecules. Meanwhile, according to our previous studies, pi-pi interactions can be formed between g-C_3N_4 and organic molecules with aromatic rings[33,34]. Among them, the pi-pi interaction can cause the organic molecules with aromatic rings to dislodge the water molecules in the compact layer to adsorb on the g-C_3N_4 surface, while the partial overlap of the wave function in space between organic molecule and g-C_3N_4 is conducive to their charge transfer. Therefore, g-C_3N_4 has general organic molecular degradation performance[31]. In contrast, the surface of $BiVO_4$ composed of terminal oxygen or hydroxyl groups is more hydrophilic, leading to stronger interactions between $BiVO_4$ and water molecules in the compact layer. Compared with water molecules, organic molecules have weaker polarity and larger volume. This results in a weaker interaction between

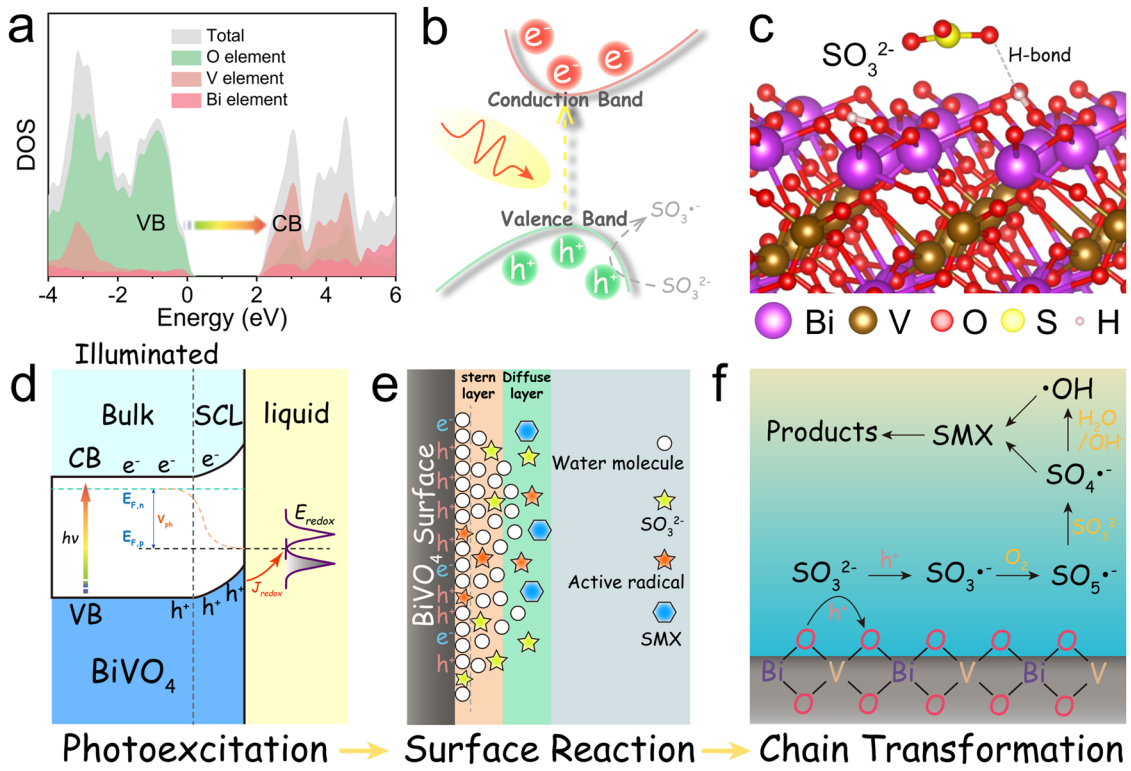

Fig. 5 Electronic structure and solid–liquid interface reaction mechanism of $BiVO_4$. **a** DOS calculation for $BiVO_4$; **b** the proposed photocatalytic decomposition process of SO_3^{2-} on the $BiVO_4$; **c** adsorption of monodentate SO_3^{2-} on the $BiVO_4$ with (110) facet; **d** quasistatic energy profile and charge transfer pathways of $BiVO_4$ under continuous illumination in contact with the aqueous solution. J_{redox} is the target charge transfer from the valence band to the redox reagent, SCL is space charge layer, V_{ph} is the open-circuit photovoltage. $E_{F,n}$ and $E_{F,p}$ are the quasi-Fermi levels of electrons and holes under illumination, respectively; **e** model of the double-layer structure of $BiVO_4$ in contact with the aqueous solution under equilibrium conditions; **f** transformation pathways of major species in $Na_2SO_3/BiVO_4$.

organic molecules and $BiVO_4$, and is not conducive to the diffusion of organic molecules from the bulk solution to the solid-liquid interface. Therefore, combined with the non-radical mechanism and surface structural features of $BiVO_4$, it is difficult for organic molecules with low polarity and high ionization potential to enter the compact layer of $BiVO_4$ and perform non-radical electron transfer. The steric segregation between organic molecules and holes triggers the deactivation of the photocatalytic system. This phenomenon is named surface solvation-induced inactivation (SSII). Compared with organic molecules, the wave function of sulfite in the form of anion is more diffuse in space, which is conducive to the formation of electrostatic interaction-dominated hydrogen bonds with the hydroxyl on the surface of $BiVO_4$ and into the compact layer. Meanwhile, sulfites with low ionization energy are favorably oxidized by the holes of $BiVO_4$ (Supplementary Tables 1 and 2), thereby promoting the generation of active species. Therefore, the introduction of sulfite realizes the indirect degradation of SMX by $BiVO_4$, which expands the steric reaction ability of $BiVO_4$ to organic molecules.

Based on above results, an overall model of $Na_2SO_3/BiVO_4$ system from photoexcitation to surface reaction is proposed. As depicted in Fig. 5d, the contact of $BiVO_4$ as an n-type semiconductor with water will lead to the formation of a space charge layer (SCL) and an upward energy band bend. When $BiVO_4$ is excited under visible light, the quasi-Fermi level of holes ($E_{F,P}$) drops significantly and generates photovoltage. Under the action of photovoltage and band bending, holes will grab electrons from substrate molecules with suitable redox potentials. Meanwhile, the $BiVO_4$ will be solvated and form double layer (including compact layer and diffuse layer) mainly composed of solvent molecules (Fig. 5e). This severely hinders the interfacial interaction and electron transfer between substrate molecules and $BiVO_4$. According to the above results, SMX can only be in the diffuse layer, while sulfite can enter the compact layer of $BiVO_4$. Once sulfite is oxidized by the hole of $BiVO_4$ with one electron, the generated $SO_3^{\bullet-}$ will then undergo chain transformation to generate active species and enter into the diffuse layer to participate in the oxidation of SMX (Fig. 5e, f).

Quantitative structure-activity relationships

In addition, the degradation of various pollutants by $Na_2SO_3/BiVO_4$ system are further investigated. According to the above results, $SO_4^{\bullet-}$ is the predominant active species in the $Na_2SO_3/BiVO_4$ system, while •OH play an auxiliary role. Among them, •OH are non-selective active species, while $SO_4^{\bullet-}$ have certain selectivity. It could be seen from Supplementary Fig. 13 that no significant degradation of phenol, aniline, and benzoic acid is observed in the $BiVO_4$ photocatalytic system. However, the concentration of nitrobenzene exhibits a significant decrease, which might originate from the reduction of the nitro group by solvated electrons diffusing out of the tight layer. In contrast, the $Na_2SO_3/BiVO_4$ system exhibited obvious photocatalytic degradation performance for various pollutants (Fig. 6a). Wherein, aromatic compounds with electron-donating substituents (phenol and aniline) present better degradation rate, while aromatic compounds with electron-withdrawing groups (benzoic acid and nitrobenzene) are more difficult to be degraded. To further explore the reasons for the differences in the degradation performance of various pollutants, a correlation between the adiabatic ionization potential (AIP) of organic molecules and the rate constant (k) is constructed. Generally, AIP can be used to

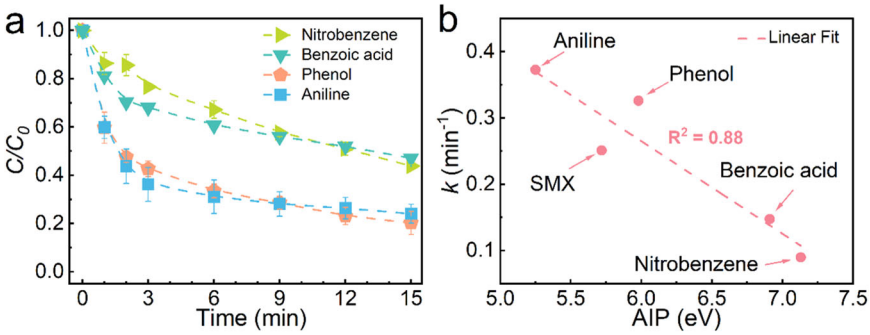

Fig. 6 Quantitative structure-activity relationship. Degradation performance for **a** monosubstituted benzenes; **b** relationship between the *k* and AIP value. Experimental condition: [organic] = 4 μM, [Na_2SO_3] = 0.50 mM, [$BiVO_4$] = 1.0 g L^{-1}, initial pH = 7.0, $\lambda \geq 420$ nm, and $T = 25$ °C. The center of the data point is the mean of the two sets of data, and error bars represent the standard deviation of the two sets of data.

describe the tendency of organic molecules to lose electrons, which is similar to the electron transfer in the oxidation of organic compounds by active species. As delineated in Fig. 6b, there is a good linear correlation between *k* and the AIP of various pollutants. In conclusion, $Na_2SO_3/BiVO_4$ system is more inclined to the degradation of electron-rich organics, indicating the structure-dependent degradation of organic molecules.

DISCUSSION

In this work, the oxidation kinetics of organic molecular controlled by the solid-liquid interface in the $BiVO_4$ photocatalytic system is revealed. Initially, the holes belong to short-range active species and are localized on the photocatalyst surface. Meanwhile, the generation of solid–liquid interface in the actual system triggers the spatial isolation between the photocatalyst and the organic molecules, which leads to the deactivation of the degradation of organic molecules on the surface of $BiVO_4$. However, sulfites with lower AIP and higher adsorption energy on the surface of $BiVO_4$ can accumulate in the compact layer of $BiVO_4$ and trap the generated photogenerated hole for single-electron oxidation. The generated sulfite radical undergoes chain transformation under the induction of oxygen to generate active species ($SO_4^{\bullet-}$) to degrade SMX. This results in a sulfite-mediated indirect electron transfer from SMX to $BiVO_4$. A model of $Na_2SO_3/BiVO_4$ system from photocatalyst excitation to interface reaction is established. In addition, there is a good linear correlation between the rate constant (*k*) and AIP of various pollutants in the $Na_2SO_3/BiVO_4$ system, indicating the structure-dependence of organic molecules degradation. This study provides insight for further understanding the effect of solid-liquid interface on reaction kinetics in heterogeneous photocatalytic system.

METHODS

Chemicals and materials

Sources of chemicals and materials are provided in Supplementary Method 1.

Preparation of $BiVO_4$

Bismuth vanadate ($BiVO_4$) was synthesized by a hydrothermal method as reported in the literature[35]. Typically, 12 mmol $Bi(NO_3)_3 \cdot 5H_2O$ was dissolved into 64 mL of 1 M HNO_3. After stirring for 0.5 h, 12 mmol NH_4VO_3, and 0.1 mol urea were quickly poured into the above solutions, and the color of the precipitate gradually changed from blood red to bright yellow. Subsequently, the beaker was placed in an 80 °C oil bath for 24 h with magnetic stirring. After natural cooling, the yellow precipitation was collected by centrifugation, washed with ethanol (EtOH) and water repeatedly, and then dried at 60 °C overnight.

Experimental procedure

Batch experiments were carried out in a 100 mL glass beaker at 25 °C under magnetic stirring. In a typical test, 50 mg of $BiVO_4$ was ultrasonically dispersed into the beaker containing 50 mL of 4 μM SMX, and then a certain mass of Na_2SO_3 was introduced under magnetic stirring. Subsequently, the initial pH was adjusted to 7.0 by using 0.05 M H_2SO_4 or NaOH. Meanwhile, the Xenon lamp (CEL-HXF300, Beijing China Education Au-light Co., Ltd) equipped with 420 nm cutoff filter was preheated at least 30 min to ensure the stability of the light source, and then the light intensity was adjusted to 400 mW cm^{-2} using an optical power meter (CEL-NP2000-10A, Beijing China Education Au-light Co., Ltd). At certain time intervals, 800 μL of the reacting solution was withdrawn, mixed with 800 μL of methanol to quench reactive species, filtered through a 0.22 μm PTFE filter, and then for further analysis. All experiments were conducted in duplicates at least, and the averaged values with standard deviations were reported.

Analytical methods

The concentration of organics was quantified by on a Waters e2695 equipped with a C18 column and a UV-vis detector with details shown in Supplementary Table 3. The pH values were monitored by a Shanghai Leici pH meter with daily calibration. The concentration of dissolved oxygen (DO) was measured by a JPB-607A portable meter (Leici, Shanghai, China). ESR signals of radical spin-trapped with 5,5-dimethyl-1-pyrroline N-oxide (DMPO) were obtained using a JES-FA200 (JEOL Co., USA) spectrometer equipped with a 300 W Xe lamp (420 nm filter) as visible light source. The material characterization techniques, trapping experiments, and photoelectrochemical measurements are given in the Supplementary Information (Supplementary Method 2–4).

Density functional theory (DFT) calculation analysis

The theoretical calculations of isolated and periodic systems were performed by Quantum Espresso (QE 6.5), Gaussian 16 C.01, and CP2K 9.1, respectively[36–39]. The CP2K 9.1 input file was generated through Multiwfn 3.8_dev[40]. Details on DFT calculation can be found in Supplementary Method 5.

DATA AVAILABILITY

The data that support the findings of this study are available from the corresponding author upon reasonable request.

Received: 31 December 2022; Accepted: 2 May 2023;
Published online: 20 May 2023

REFERENCES

1. Loeb, S. K. et al. The technology horizon for photocatalytic water treatment: sunrise or sunset? *Environ. Sci. Technol.* **53**, 2937–2947 (2019).
2. Hoffmann, M. R., Martin, S. T., Choi, W. & Bahnemann, D. W. Environmental applications of semiconductor photocatalysis. *Chem. Rev.* **95**, 69–96 (1995).
3. Yang, Z. et al. Toward selective oxidation of contaminants in aqueous systems. *Environ. Sci. Technol.* **55**, 14494–14514 (2021).
4. Chen, F. et al. Catalytic degradation of ciprofloxacin by a visible-light-assisted peroxymonosulfate activation system: performance and mechanism. *Water Res.* **173**, 115559 (2020).
5. Jiang, R. et al. Fabrication of Fe_3O_4 quantum dots modified BiOCl/$BiVO_4$ p-n heterojunction to enhance photocatalytic activity for removing broad-spectrum antibiotics under visible light. *J. Taiwan Inst. Chem. Eng.* **96**, 681–690 (2019).
6. Long, M. et al. EfficienT PHOTOCATALYTIC DEGRADATION OF PHENOL over Co_3O_4/$BiVO_4$ composite under visible light irradiation. *J. Phys. Chem. B* **110**, 20211–20216 (2006).
7. Zhang, Z., Wang, W., Shang, M. & Yin, W. Photocatalytic degradation of rhodamine B and phenol by solution combustion synthesized $BiVO_4$ photocatalyst. *Catal. Commun.* **11**, 982–986 (2010).
8. Tan, H. L., Amal, R. & Ng, Y. H. Alternative strategies in improving the photocatalytic and photoelectrochemical activities of visible light-driven $BiVO_4$: a review. *J. Mater. Chem. A* **5**, 16498–16521 (2017).
9. He, S., Chen, Y., Li, X., Zeng, L. & Zhu, M. Heterogeneous photocatalytic activation of persulfate for the removal of organic contaminants in water: a critical review. *ACS EST Eng.* **2**, 527–546 (2022).
10. Chen, J., Zhou, X., Sun, P., Zhang, Y. & Huang, C. H. Complexation enhancees Cu(II)-activated peroxydisulfate: a novel activation mechanism and Cu(III) contribution. *Environ. Sci. Technol.* **53**, 11774–11782 (2019).
11. Li, H., Shan, C. & Pan, B. Fe(III)-Doped g-C_3N_4 mediated peroxymonosulfate activation for selective degradation of phenolic compounds via high-valent iron-oxo species. *Environ. Sci. Technol.* **52**, 2197–2205 (2018).
12. Zong, Y. et al. Unraveling the overlooked involvement of high-valent cobalt-oxo species generated from the cobalt(ii)-activated peroxymonosulfate process. *Environ. Sci. Technol.* **54**, 16231–16239 (2020).
13. Li, Y., Zhang, W., Niu, J. & Chen, Y. Mechanism of photogenerated reactive oxygen species and correlation with the antibacterial properties of engineered metal-oxide nanoparticles. *ACS Nano* **6**, 5164–5173 (2012).
14. Wang, Z. et al. Aqueous iron(IV)-oxo complex: an emerging powerful reactive oxidant formed by iron(ii)-based advanced oxidation processes for oxidative water treatment. *Environ. Sci. Technol.* **56**, 1492–1509 (2022).
15. Crespo-Otero, R. & Walsh, A. Variation in surface ionization potentials of pristine and hydrated $BiVO_4$. *J. Phys. Chem. Lett.* **6**, 2379–2383 (2015).
16. Wang, W. et al. Influence of excess charge on water adsorption on the $BiVO_4$ (010) surface. *J. Am. Chem. Soc.* **144**, 17173–17185 (2022).
17. Wiktor, J. & Pasquarello, A. Electron and hole polarons at the $BiVO_4$–water interface. *ACS Appl. Mater. Inter.* **11**, 18423–18426 (2019).
18. Wu, S., Shen, L., Lin, Y., Yin, K. & Yang, C. Sulfite-based advanced oxidation and reduction processes for water treatment. *Chem. Eng. J.* **414**, 128872 (2021).
19. Chong, M. N., Jin, B., Chow, C. W. & Saint, C. Recent developments in photocatalytic water treatment technology: a review. *Water Res.* **44**, 2997–3027 (2010).
20. Deng, W. et al. Visible-light-driven photocatalytic degradation of organic water pollutants promoted by sulfite addition. *Environ. Sci. Technol.* **51**, 13372–13379 (2017).
21. Wei, Y. et al. Photocatalytic degradation of organic pollutants in wastewater with g-C_3N_4/sulfite system under visible light irradiation. *Chemosphere* **208**, 358–365 (2018).
22. Gao, X. et al. New insight into the mechanism of symmetry-breaking charge separation induced high-valent iron(IV) for highly efficient photodegradation of organic pollutants. *Appl. Catal. B: Environ.* **321**, 122066 (2023).
23. Rao, D. et al. New mechanistic insights into the transformation of reactive oxidizing species in an ultraviolet/sulfite system under aerobic conditions: modeling and the impact of Mn(II). *ACS EST Water* **1**, 1785–1795 (2021).
24. Chen, H. et al. Novel solar/sulfite advanced oxidation process for carbamazepine degradation: radical chemistry, transformation pathways, influence on disinfection byproducts and toxic changes. *Chem. Eng. J.* **451**, 138634 (2023).
25. Wang, Z. et al. Is sulfate radical really generated from peroxydisulfate activated by iron(II) for environmental decontamination? *Environ. Sci. Technol.* **52**, 11276–11284 (2018).
26. Liang, J. et al. Persulfate oxidation of sulfamethoxazole by magnetic iron-char composites via nonradical pathways: Fe(IV) versus surface-mediated electron transfer. *Environ. Sci. Technol.* **55**, 10077–10086 (2021).
27. Wetchakun, N. et al. $BiVO_4$/CeO_2 nanocomposites with high visible-light-induced photocatalytic activity. *ACS Appl. Mater. Inter.* **4**, 3718–3723 (2012).
28. Cooper, J. K. et al. Electronic structure of monoclinic $BiVO_4$. *Chem. Mater.* **26**, 5365–5373 (2014).
29. Che, H. et al. Rational design of donor-acceptor conjugated polymers with high performance on peroxydisulfate activation for pollutants degradation. *Appl. Catal. B: Environ.* **316**, 121611 (2022).
30. Wang, D., Chen, J., Gao, X., Ao, Y. & Wang, P. Maximizing the utilization of photogenerated electrons and holes of g-C_3N_4 photocatalyst for harmful algae inactivation. *Chem. Eng. J.* **431**, 134105 (2022).
31. Gao, X., Chen, J., Che, H., Ao, Y. & Wang, P. Rationally constructing of a novel composite photocatalyst with multi charge transfer channels for highly efficient sulfamethoxazole elimination: Mechanism, degradation pathway and DFT calculation. *Chem. Eng. J.* **426**, 131585 (2021).
32. Che, H. N. et al. Iodide-induced fragmentation of polymerized hydrophilic carbon nitride for high-performance quasi-homogeneous photocatalytic H_2O_2 production. *Angew. Chem. Int. Ed.* **60**, 25546–25550 (2021).
33. Zhang, Q. et al. Understanding the mechanism of interfacial interaction enhancing photodegradation rate of pollutants at molecular level: Intermolecular pi-pi interactions favor electrons delivery. *J. Hazard. Mater.* **430**, 128386 (2022).
34. Zhang, Q. et al. In-depth insight into the mechanism on photocatalytic synergistic removal of antibiotics and Cr (VI): the decisive effect of antibiotic molecular structure. *Appl. Catal. B Environ.* **313**, 121443 (2022).
35. Gao, X., Ma, C., Liu, Y., Xing, L. & Yan, Y. Self-induced Fenton reaction constructed by Fe(III) grafted $BiVO_4$ nanosheets with improved photocatalytic performance and mechanism insight. *Appl. Surf. Sci.* **467-468**, 673–683 (2019).
36. Giannozzi, P. et al. QUANTUM ESPRESSO: a modular and open-source software project for quantum simulations of materials. *J. Phys. Condens. Matter* **21**, 395502 (2009).
37. Giannozzi, P. et al. Advanced capabilities for materials modelling with Quantum ESPRESSO. *J. Phys. Condens. Matter* **29**, 465901 (2017).
38. Frisch, M. J. et al. Gaussian 16 Rev. C.01, *Gaussian, Inc.* (2016).
39. Kühne, T. D. et al. CP2K: an electronic structure and molecular dynamics software package-Quickstep: Efficient and accurate electronic structure calculations. *J. Chem. Phys.* **152**, 194103 (2020).
40. Lu, T. & Chen, F. Multiwfn: a multifunctional wavefunction analyzer. *J. Comput. Chem.* **33**, 580–592 (2012).

ACKNOWLEDGEMENTS

We are grateful for grants from the Natural Science Foundation of China (51979081, 52100179), Fundamental Research Funds for the Central Universities(B200202103), National Science Funds for Creative Research Groups of China (No. 51421006), PAPD, and Postgraduate Research & Practice Innovation Program of Jiangsu Province (KYCX22_0680).

AUTHOR CONTRIBUTIONS

X.G.: methodology, software, validation, visualization, calculation, writing – original draft. H.C.: methodology, software, validation, visualization. W.L.: writing – review & editing, formal analysis. P.W.: formal analysis, writing – review & editing. Y.A.: conceptualization, writing – review & editing, supervision, funding acquisition, validation, formal analysis.

COMPETING INTERESTS

The authors declare no competing interests.

ADDITIONAL INFORMATION

Supplementary information The online version contains supplementary material available at https://doi.org/10.1038/s41545-023-00254-w.

Correspondence and requests for materials should be addressed to Peifang Wang or Yanhui Ao.